Available online at www.sciencedirect.com
ScienceDirect
International Journal of Heat and Mass Transfer 50 (2007) 2816–2827
International Journal of HEAT and MASS TRANSFER
www.elsevier.com/locate/ijhmt

Analysis of the heat transfer of an impinging laminar flame jet

M.J. Remie, M.F.G. Cremers, K.R.A.M. Schreel, L.P.H. de Goey *

Eindhoven University of Technology, Department of Mechanical Engineering, P.O. Box 513, 5600 MB Eindhoven, The Netherlands

Received 8 September 2005; received in revised form 23 May 2006
Available online 6 March 2007

Abstract

Flame jet impingement is used in many industrial processes. In this paper an analytical expression is derived for the heat flux of a laminar flame impinging on a flat plate, where the flame jet is approximated by a hot inert jet with the position of the tip of the flame taken equal to the nozzle position. The heal flux in this expression is dependent on the nozzle-to-plate spacing, in contradiction to existing (semi-analytical) relations. The geometry is divided in a region far from the plate and a region dose to the plate. For both regions the velocity profiles are calculated using only the dominant terms of the balance equations. Subsequently these profiles are linked to each other at the boundary between the two zones. Implementing the resulting velocity profile for the complete geometry in the energy equation and integrating over the whole domain results in an expression for the heat flux from the flame to the plate at the hot spot. Numerical calculations show very good agreement with the results of the analytical derivation.

Keywords: Impinging flame jet; Heat transfer; Strain

1. Introduction

Jet impingement is widely used in industrial applications where high convective heat transfer rates are required. Applications include drying of textiles, film and paper, cooling of turbine blades and microelectric components and heating of glass products. It is well reckoned that these jets yield very high heat transfer coefficients. A lot of work is documented on flow behaviour and heat transfer of jets. Li et al. [1] showed that there exist two different solutions for the flow field in some range of geometric and flow parameters. The use of multiple jets results in a wider range in heat transfer rates and distributions. Aldabbagh and Sezai described the flow behaviour of multiple impinging jets numerically [2], while Geers performed experiments on flow and heat transfer [3].

Impinging jets are operated in a laminar as well as a turbulent configuration. An impinging jet is observed to be laminar up to a Reynolds number of approximately 2500, based on the nozzle diameter width. Turbulent impinging jets are observed to yield a higher heat transfer than laminar jets [4]. Wang and Mujumdar [5] compared several k–ε models for the prediction of the heat transfer of turbulent impinging jets. Angioletti et al. [6] compared several turbulence models with PIV measurements. Although turbulent jets are more often encountered in industrial applications, the jets will be laminar for smaller geometries or viscous fluids. A special case of jets are small flame jets, which are used in the glass and steel industry where the heat has to be applied locally for cutting and melting purposes. These flows are highly viscous because of their high temperatures. Since these flames are laminar, mixing of ambient air causing a temperature decrease of the flame is suppressed.

In the last few decades it became more accepted to increase the amount of oxygen in these flame jets. Enhancing the amount of oxygen in flame jets is adopted to increase metal heating and melting rates because of the higher flame temperature (2300 K for methane–air flames, 3000 K for methane–oxygen flames) and higher gas velocity [7,8]. Oxygen-enhanced combustion considerably alters

* Corresponding author. Tel.: +31 40 2472140; fax: +31 40 2433445.
E-mail address: l.p.h.d.goey@tue.nl (L.P.H. de Goey).

0017-9310/$ - see front matter © 2007 Elsevier Ltd. All rights reserved.
doi:10.1016/j.ijheatmasstransfer.2006.10.053

Nomenclature

a	strain rate before the plate [1/s]
c_p	specific heat at constant pressure [J/(kg K)]
$\mathbf{g}$	gravitational vector [m/s^2]
h	distance burner nozzle to plate [m]
H	distance flame tip to plate [m]
$\mathbf{I}$	unit tensor
K	strain rate [1/s]
$\dot{m}$	mass flow [kg/(m^2 s)]
p	pressure [Pa]
$\mathscr{P}$	stress tensor [kg/(m^2 s)]
Pr	Prandtl number (ν/α)
Pe	Peclet number (UH/α)
q	heat flux [W/m^2]
r	cylindrical coordinate
R	radius of the plug flow [m]
t	time [s]
T	temperature [K]
u, v	Cartesian velocities [m/s]
U	velocity of the plug flow [m/s]
$\mathbf{v}$	velocity vector [m/s]
x, y	Cartesian coordinates [m]
x_δ	viscous boundary layer thickness [m]

Greek symbols

α	thermal diffusivity [m^2/s]
λ	conductivity coefficient [W/(m K)]
μ	dynamic viscosity [kg/(m s)]
ν	kinematic viscosity [m^2/s]
ρ	density [kg/m^3]
τ	stress tensor [kg/(m^2 s)]

Subscript

b	burnt

the value and location of the peak heat flux. Baukal and Gebhart [9] experimentally found that the heat flux to the target increased by as much as 230% as the fraction of oxygen increased from 0.30 to 1.00 in the oxidizer stream. Furthermore, the peak heat flux did not occur at the stagnation point for low oxidizer compositions. At high values of the oxidizer composition however, the peak heat flux did occur at the stagnation point. The increased heat transfer is the main reason that nowadays the flame jets are operated with pure oxygen instead of air.

The flow behaviour of flame jets and hot isothermal jets is comparable. According to Viskanta [4], the aerodynamics of a single flame jet is very similar to the aerodynamics of a single isothermal jet. Experiments by Van der Meer [10] showed that the axial velocity decays slightly faster for the flame jets than for the isothermal jets, due to the axial temperature decay. The radial velocity gradients at the stagnation point are found to be equal. Most studies concern the stationary flame impinging on a (flat) surface. Tuttle et al. [11,12] however examined the unsteady characteristics of the impingement heat transfer. Lately, research has been performed by Dong et al. [13,14] and Kwok et al. [15,16] concerning the heat transfer characteristics of single and multiple impinging flame jets and slot and round impinging flame jets. Zhao et al. [17] found that the thermal conductivity of the impingement plate provides the major influence on the heat transfer from the flame jet to the plate. Since the flow behaviours of flame jets and hot isothermal jets are comparable, we will focus on isothermal jets in the rest of this paper.

One big difference however exists between flame jets and isothermal jets if we look at the heat transfer mechanisms for these jets. The main heat transfer mechanism for impinging flame jets is forced convection. Increasing the oxidizer composition results in a higher flame temperature and burning velocity and therefore a higher gas velocity. Not only forced convection will be enlarged, but the heat transfer mechanism called thermochemical heat release starts to play an important role [18]. These flames contain a lot of free radicals such as O, H and OH. When these radicals enter the cold boundary layer, they exothermically recombine and augment the heat transfer. This process has also been called chemical recombination or convection vivre. Cremers et al. [19] found that this mechanism for a hydrogen–oxygen flame causes a heat transfer coefficient which is twice as high as the heat transfer coefficient for a chemically frozen mixture. It is clear that chemical recombination, which is not present in an isothermal jet, therefore has a big influence on the heat transfer of a flame jet.

The influence of radiation is very small. According to Van der Meer [10], the radiation of the flame is negligible because of the very low emissivity of a hot gas layer of small thickness. Baukal and Gebhart [18] and Viskanta [4] also confirmed the minor role of nonluminous radiation.

Although a lot of work is performed on measuring the heat flux from flame jets to a (flat) surface, simple analytical expressions for this heat flux are still lacking. From an engineering point of view, such an expression is very useful when the heat flux from an impinging flame to a product needs to be estimated. In this paper, we will derive an analytical expression for the heat flux from a flame jet to a flat plate, where the flame jet is approximated by a hot isothermal jet. The effect of chemical recombination is not taken into account. How to involve this effect in the analysis will be further looked upon in the future.

Heat transfer from an inert jet to a plate has been studied extensively in the past [20–23]. Sibulkin derived a semi-analytical relation for the laminar heat transfer of an impinging flow to a body of revolution [20], which has been

the basis of most other experimental and theoretical results since. An important parameter in this relation is the velocity gradient just outside the boundary layer. This velocity gradient is a function of the nozzle diameter and the free-stream velocity, but not of the nozzle-to-plate spacing. In the analytical solution we present here, the dependence of the nozzle-to-plate spacing is incorporated.

First the physical configuration is analysed. A sketch of a flame impinging on a plane surface is shown in Fig. 1. Four characteristic regions can be distinguished, namely the flame region, the free jet region, the stagnation region and the wall jet region. We assume in our analysis that a plug flow with velocity U and width $2R$ is formed after the burnt gases have expanded behind the flame front. Experiments in our laboratory indeed show that a plug flow is formed after the flame front for fuel–oxygen flames. At the edges of the stream tube the velocity of the burnt gases will rapidly drop. In literature often the distance from the nozzle to the impingement surface h is used as an independent parameter, for inert as well as flame jets. However, using different fuels while keeping the unburnt gas velocity constant results in different flame heights because of the different burning velocities. Therefore, if the distance from the burner to the plate h is kept constant, the distance from the flame tip to the plate H will vary for the different fuels. For this reason, we choose the distance from the flame tip to the plate H as an input parameter, instead of the distance from the burner to the plate h. Furthermore it is assumed that the to be heated product is placed close to the flame front, compared with the width of the burnt gas flow ($H < 2R$). The configuration therefore reduces to an effective one-dimensional problem and can be approached as an isothermal stagnation flow impinging on a flat surface. An analytical approximation for the heat flux to the hot spot in this configuration is assessed, where the width of the hot spot is equal to $2R$. The resulting expression can be used to calculate the local heat flux, which is of practical interest for cutting and melting purposes. It has to be stated that the globally transferred heat of a single jet is not calculated. However, the solution is also applicable for a closely staggered array of holes. The approximation is done for a two-dimensional as well as a cylinder-symmetrical case by solving the conservation equations taking only the most important contributions into account. It is not possible to find the full analytical solution even though the system is one-dimensional. The results are therefore validated by numerical calculations using Fluent [24].

2. Analytical solution for the heat transfer for a two-dimensional case

For the case of small distances of the flame to the plate, $H < 2R$, the situation effectively reduces to a steady one-dimensional problem. Fig. 2 represents the situation, the directions for x, y, u and v are chosen according to the figure. The unburnt gases flow out of a burner nozzle, whereupon a plug flow is formed after the flame front. The system behaves as an isothermal potential flow far from the surface, with a thin boundary layer of thickness x_δ close to the surface, where heat transfer processes induce a fast temperature change. The system is analysed by studying the transport equations in both regions and coupling the solutions at the edge of the regions.

We start from the conservation equations of mass and momentum:

$$\frac{\partial \rho}{\partial t} + \nabla \cdot (\rho \mathbf{v}) = 0, \tag{1}$$

$$\frac{\partial (\rho \mathbf{v})}{\partial t} + \nabla \cdot (\rho \mathbf{v}\mathbf{v}) = -\nabla \cdot \mathscr{P} + \rho \mathbf{g}, \tag{2}$$

where $\mathbf{g}$ is the gravitational vector [m/s^2] and the tensor $\mathscr{P}$ is a short-hand notation for $\mathscr{P} = p\mathbf{I} + \tau$. Furthermore, p is the hydrostatic pressure [Pa], $\mathbf{I}$ the unit tensor and τ the stress-tensor [kg/(m s^2)].

Often the Richardson number Ri is used to determine the importance of buoyancy in the flow. The Richardson number is a dimensionless number that expresses the ratio of potential to kinetic energy. Since $Ri = \mathcal{O}(10^{-5})$ in this case, the effect of buoyancy is neglected. The jet is inert,

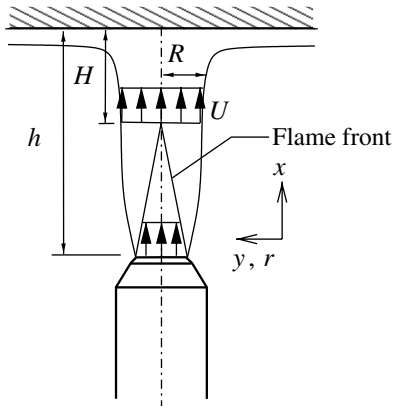

Fig. 1. Flame impinging normal to a plane surface.

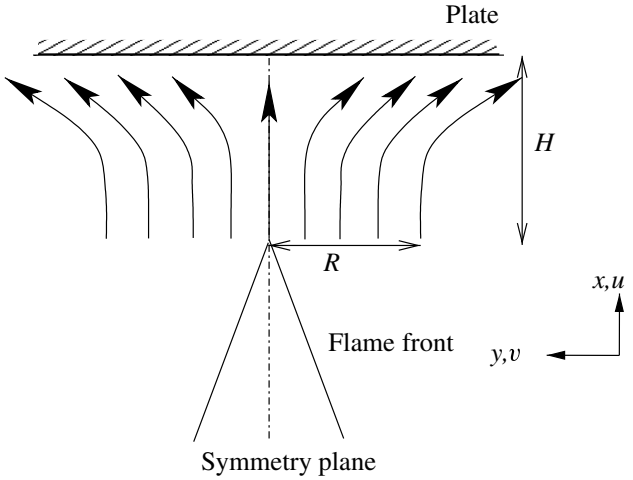

Fig. 2. Schematic overview of a 2D stagnation flame.

since we approximate the flame jet by a hot isothermal jet and take no chemical recombination into account. We assume that the temperature is a function of the spatial coordinate x only, so $T = T(x)$ and therefore $\rho = \rho(x)$. Assuming an incompressible flow and using the ideal gas law $p = \rho RT$, ρT is a constant. The continuity equation now yields

$$\frac{\partial(\rho u)}{\partial x} = -\rho\frac{\partial v}{\partial y} = -\rho K, \tag{3}$$

where $K = \frac{\partial v}{\partial y}$.

If Eqs. (1) and (2) are applied to a region close to the symmetry plane, the velocity component u will be a function of x only. Therefore, K is a function of x only. Using $\dot{m} = \rho u$ and $p = p(x, y)$, $v = y \cdot \hat{v}(x)$ and $\mu = \mu(x)$, the following conservation equations for mass and x- and y-momentum now hold [25,26]:

$$\frac{\mathrm{d}\dot{m}}{\mathrm{d}x} = -\rho K, \tag{4}$$

$$\frac{\partial p}{\partial x} = -\dot{m}\frac{\mathrm{d}u}{\mathrm{d}x} + \frac{\mathrm{d}}{\mathrm{d}x}\left[\frac{2}{3}\mu\left(2\frac{\mathrm{d}u}{\mathrm{d}x} - K\right)\right] + \mu\frac{\mathrm{d}K}{\mathrm{d}x}, \tag{5}$$

$$\dot{m}\frac{\mathrm{d}K}{\mathrm{d}x} + \rho K^2 - \frac{\mathrm{d}}{\mathrm{d}x}\left(\mu\frac{\mathrm{d}K}{\mathrm{d}x}\right) = -\frac{1}{y}\frac{\mathrm{d}p}{\mathrm{d}y}, \tag{6}$$

with μ the dynamic viscosity [kg/(m s)]. It can be seen from Eq. (5), that the pressure derivative $\partial p/\partial x$ is a function of x only. Differentiation of Eq. (5) with respect to y and changing the order of differentiation then gives that $\partial p/\partial y$ is a function of y only. From Eq. (6) it then follows that $-\frac{1}{y}\frac{\mathrm{d}p}{\mathrm{d}y}$ is a constant, i.e.

$$\dot{m}\frac{\mathrm{d}K}{\mathrm{d}x} - \frac{\mathrm{d}}{\mathrm{d}x}\left(\mu\frac{\mathrm{d}K}{\mathrm{d}x}\right) = J - \rho K^2, \tag{7}$$

with $J = -\frac{1}{y}\frac{\mathrm{d}p}{\mathrm{d}y}$. Since this equation should also hold far from the plate where $\frac{\mathrm{d}K}{\mathrm{d}x} = 0$ and $\frac{\mathrm{d}^2K}{\mathrm{d}x^2} = 0, J$ must be equal to $\rho_b a^2$, where a is the strain rate in the free flow and ρ_b the density of the burnt gases behind the flame front.

Now the relation for the velocity field far from the plate to the viscous boundary layer, $-H < x < -x_\delta$, will be derived. After this, we will derive the relation for the velocity close to the plate $-x_\delta < x < 0$ and link the obtained relations to each other at the edge of the viscous boundary layer $x = -x_\delta$, see Fig. 3. If we estimate the order of magnitude far from the plate with $\mathcal{O}(x) = H, \mathcal{O}(K) = U/H$, and use Eq. (7), we obtain:

$$\mathcal{O}\left(\rho\frac{U^2}{H^2}\right) + \mathcal{O}\left(\mu\frac{U}{H^3}\right) = \mathcal{O}(\rho a^2) + \mathcal{O}\left(\rho\frac{U^2}{H^2}\right). \tag{8}$$

Since $\mathcal{O}(a) = U/H$, it is easy to see that the viscous term is not relevant far from the plate if $H \gg \sqrt{\nu/a}$, where ν is the kinematic viscosity [m^2/s]. The following equation for the velocity needs to be solved then:

$$-uu'' = a^2 - u'^2. \tag{9}$$

The temperature remains constant far from the plate and rapidly decreases close to the plate. Therefore far from the plate $u' = \frac{\partial u}{\partial x} = -K$, since $\rho\frac{\partial u}{\partial x} \gg u\frac{\partial \rho}{\partial x}$ and ρT is a constant.

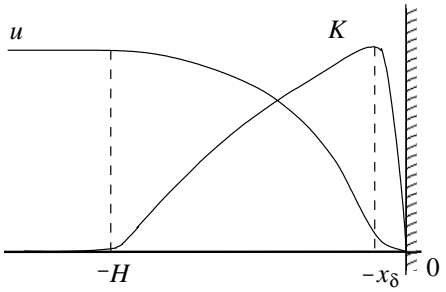

Fig. 3. Velocity and strain profile of the burnt gases.

The boundary conditions follow from Fig. 3. At $x = -H$, $u = U$ and $K = 0$.

The solution is given by

$$u(x) = U\sin\left(\frac{-ax + x_{\mathrm{ref}}}{U}\right), \tag{10}$$

where $a = \frac{\pi U}{2H}$ and the value of x_{ref} is determined by the boundary layer thickness x_δ. Furthermore,

$$K(x) = a\cos\left(\frac{-ax + x_{\mathrm{ref}}}{U}\right). \tag{11}$$

Eqs. (10) and (11) are valid for $-H < x < -x_\delta$, but also for the whole domain if the flow is non-viscous ($x_{\mathrm{ref}} = 0$). Close to the plate, $-x_\delta < x < 0$, the terms $\dot{m}\frac{\mathrm{d}K}{\mathrm{d}x}$ and ρK^2 from Eq. (7) become zero close to the wall, so for $x \simeq 0$ and constant viscosity, Eq. (7) can be approximated by

$$-\mu\frac{\mathrm{d}^2K}{\mathrm{d}x^2} = \rho_b a^2, \tag{12}$$

indicating a quadratic behaviour as function of x for K in the viscous boundary layer.

At $x = -x_\delta$ the strain rate K is maximum and equal to $a \simeq \frac{\pi U}{2H}$. Using this boundary condition and $K(0) = 0$, the strain rate K in the viscous boundary layer can be calculated. Close to the plate, the density and velocity of the burnt gas flow can be approximated by

$$\rho \sim \rho_0 + \rho' x, \quad u \sim bx^2,$$

with ρ_0 the density of the burnt gas flow at the flame side of the plate and b a constant. Since

$$\rho\frac{\mathrm{d}u}{\mathrm{d}x} \sim 2b\rho_0 x, \quad u\frac{\mathrm{d}\rho}{\mathrm{d}x} \sim b\rho' x^2,$$

and therefore $\rho \mathrm{d}u/\mathrm{d}x \gg u\mathrm{d}\rho/\mathrm{d}x$, the strain rate can be approximated by $K(x) = -\frac{\partial u}{\partial x}$.

The velocity solution in the boundary layer equals:

$$u(x) = ax_\delta\left(\frac{x^3}{3x_\delta^3} + \frac{x^2}{x_\delta^2}\right), \tag{13}$$

with $x_\delta = \sqrt{2\mu/(\rho a)} = \sqrt{2\nu/a}$. The relations for the velocity, Eqs. (10) and (13) are linked by the condition that the strain rate at $x = -x_\delta$ must equal $K = a = \frac{\pi U}{2H}$. Now x_{ref} can be calculated and Eq. (10) becomes:

$$u(x) = U \sin\left(\frac{-a(x + x_\delta/3)}{U}\right). \tag{14}$$

The relation for the heat flux to the plate can be derived if we consider the energy equation of the burnt gases close to the heated side of the plate. The heat flux can be calculated via a balance of conduction and convection. The conservation equation is given by

$$\rho u c_p \frac{\partial T}{\partial x} = \frac{\partial}{\partial x}\left(\lambda \frac{\partial T}{\partial x}\right), \tag{15}$$

where c_p is the heat capacity of the burnt gas flow [J/(kg K)] and λ the conductivity coefficient [W/(m K)]. Substituting the equations for the velocity u results in relations for the heat transfer from the burnt gas flow to the glass product. First we determine the heat transfer for a non-viscous gas flow ($x_\delta = 0$). We assume that λ is constant and $\alpha = \frac{\lambda}{\rho c_p}$, with α the thermal diffusivity [m^2/s], is constant as well. Numerical calculations indeed show that α can be considered constant. After substituting Eq. (10) for the velocity u and integrating x from $-H$ to 0, the heat transfer is given by

$$q = \lambda \left.\frac{\partial T}{\partial x}\right|_0 = \frac{\lambda(T_{(0)} - T_{\text{flame}})}{H \int_{-1}^{0} \exp\left[\frac{2}{\pi} Pe\left(\cos\left(-\frac{\pi}{2}x'\right) - 1\right)\right] \mathrm{d}x'}, \tag{16}$$

with $T_{(0)}$ the temperature at the hot side of the plate, x' a dimensionless coordinate defined by $x' = x/H$ and Pe the Peclet number. The Peclet number is a dimension-less parameter giving the ratio of heat transfer by convection and conduction:

$$Pe = \frac{UH}{\alpha} = \frac{UH\rho c_p}{\lambda}, \tag{17}$$

For this case, the integral in the denominator of Eq. (16) can be simplified using a Taylor expansion for the cosine. The heat transfer can be expressed as follows:

$$q = \lambda \left.\frac{\partial T}{\partial x}\right|_0 = \lambda(T_{(0)} - T_{\text{flame}}) \frac{1}{H}\sqrt{Pe}. \tag{18}$$

If we take viscosity into account to calculate the heat flux, we make a distinction between the burnt gas flow region and the viscous boundary layer again. First, we substitute the relation for the velocity in the boundary layer (13) in the energy Eq. (15) and integrate from $-x_\delta$ to 0. Next, we substitute the relation for the velocity in the burnt gas flow (14) in the energy equation and integrate from $-H$ to $-x_\delta$. The heat flux can be calculated using:

$$\begin{aligned}\int_{-H}^{0} \frac{\mathrm{d}T}{\mathrm{d}x}(s)\,\mathrm{d}s &= \int_{-H}^{0} \left.\frac{\partial T}{\partial x}\right|_0 \exp\left[-\frac{1}{\alpha}\int_s^0 u\,\mathrm{d}x\right]\mathrm{d}s \\ &= \left.\frac{\partial T}{\partial x}\right|_0 \left[\int_{-H}^{-x_\delta} \exp\left[-\frac{1}{\alpha}\left[\int_s^{-x_\delta} u_1\,\mathrm{d}x + \int_{-x_\delta}^{0} u_2\,\mathrm{d}x\right]\right]\mathrm{d}s + \int_{-x_\delta}^{0} \exp\left[-\frac{1}{\alpha}\int_s^0 u_2\,\mathrm{d}x\right]\mathrm{d}s\right],\end{aligned} \tag{19}$$

where u_1 is given by Eq. (14) and u_2 by Eq. (13). The expression for the heat flux now results in:

$$q = \lambda \left.\frac{\partial T}{\partial x}\right|_0 = \frac{\lambda(T_{(0)} - T_{\text{flame}})}{\mathscr{M}}, \tag{20}$$

with

$$\begin{aligned}\mathscr{M} = H \int_{-x_\delta/H}^{0} \exp\left[\frac{\pi^2}{96}\frac{Pe^2}{Pr}x'^4 + \frac{1}{12}\sqrt{\frac{Pe^2\pi^3}{Pr}}x'^3\right]\mathrm{d}x' \\ + H \int_{-1}^{-x_\delta/H} \exp\left[-\frac{1}{2}Pr - \frac{2}{\pi}Pe\left(\cos\left(\frac{2}{3}\sqrt{\frac{\pi Pr}{Pe}}\right) - \cos\left(-\frac{1}{3}\sqrt{\frac{\pi Pr}{Pe}} - \frac{\pi x'}{2}\right)\right)\right]\mathrm{d}x'\end{aligned} \tag{21}$$

and Pr the Prandtl number. The Prandtl number is a dimensionless number for the ratio of viscosity and thermal diffusivity: $Pr = \nu/\alpha$. In other words, an increasing Prandtl number denotes an increasing influence of viscosity and therefore a decrease of heat transfer. Note that for $Pr = 0$, the heat transfer equals Eq. (16).

3. Analytical solution for the heat transfer for a cylinder-symmetrical case

We consider Fig. 4 for the cylinder-symmetrical case, where the y-direction is replaced by the r-direction. Eqs. (1) and (2) will be applied to the symmetry plane and, since $R > H$, the velocity component u is independent of the r-direction. Again, we assume that the temperature is a function of the spatial coordinate x only, so $T = T(x)$ and therefore $\rho = \rho(x)$. Now the steady equations for conservation of mass and conservation of momentum in r-direction become:

$$\frac{\partial(\rho u)}{\partial x} + \frac{1}{r}\frac{\partial(\rho v r)}{\partial r} = 0, \tag{22}$$

$$\frac{\partial(\rho u v)}{\partial x} + \frac{1}{r}\frac{\partial(\rho v^2 r)}{\partial r} + \frac{\partial p}{\partial r} = -\frac{\partial}{\partial x}\left(-\mu\frac{\partial v}{\partial x}\right). \tag{23}$$

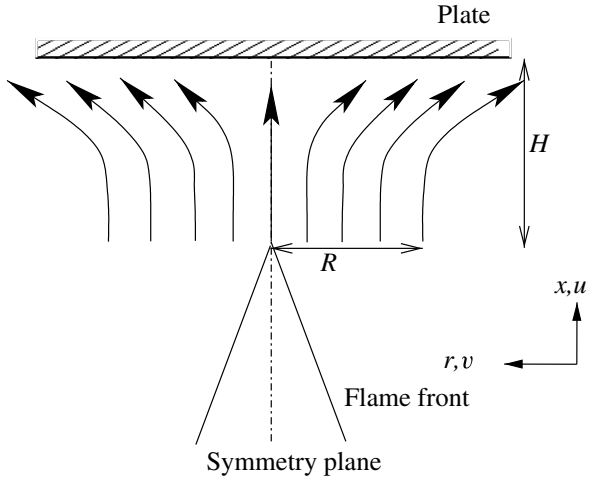

Fig. 4. Schematic overview of a cylinder-symmetrical stagnation flame.

Substituting Eq. (4) and $v = r \cdot \hat{v}(x)$ in Eq. (22) gives

$$\frac{\partial v}{\partial r} = \frac{1}{2}K. \tag{24}$$

Now, together with $\dot{m} = pu$, the equations of x- and r-momentum become [25,26]:

$$\frac{\partial p}{\partial x} = -\dot{m}\frac{\mathrm{d}u}{\mathrm{d}x} + \frac{\mathrm{d}}{\mathrm{d}x}\left[\frac{2}{3}\mu\left(2\frac{\mathrm{d}u}{\mathrm{d}x} - K\right)\right] + \frac{\mu}{2}\frac{\mathrm{d}K}{\mathrm{d}x}, \tag{25}$$

$$\dot{m}\frac{\mathrm{d}K}{\mathrm{d}x} + \frac{1}{2}\rho K^2 - 2\frac{\mathrm{d}}{\mathrm{d}x}\left(\mu\frac{\mathrm{d}\hat{v}}{\mathrm{d}x}\right) = -\frac{2}{r}\frac{\mathrm{d}p}{\mathrm{d}r}. \tag{26}$$

Analogous to the two-dimensional situation, it can be shown that $-\frac{2}{r^2}\frac{\mathrm{d}(pr)}{\mathrm{d}r}$ is a constant and equal to $\frac{1}{2}\rho_b a^2$.

Again we decouple the domain in a region consisting of the flow far from the plate to the viscous boundary layer, $-H < x < -x_\delta$, and a region consisting of the viscous boundary layer, $-x_\delta < x < 0$. The relations for the velocity will be linked at $x = -x_\delta$. Since the viscous term is not relevant far from the plate, the following equation for the velocity for $-H < x < -x_\delta$ needs to be solved:

$$-uu'' = \frac{1}{2}a^2 - \frac{1}{2}u'^2. \tag{27}$$

The same boundary conditions as for the two-dimensional case are used, see Fig. 3. The equations for the velocity and the strain rate are now given by:

$$u(x) = U - U\left(\frac{a(x + x_{\mathrm{ref}})}{2U} + 1\right)^2, \tag{28}$$

$$K(x) = a\left(\frac{a(x + x_{\mathrm{ref}})}{2U} + 1\right), \tag{29}$$

where $a = 2U/H$. Comparing this result with the two-dimensional case, the strain rate for the axisymmetrical case is a factor $4/\pi$ larger for the same burnt gas velocity U and distance from the flame front to the plate H. Since the diverging gases have more directions to flow away from the axis, the strain rate should be higher indeed.

Close to the plate, $\dot{m}$ and K become zero and Eq. (26) can be approximated for $-x_\delta < x < 0$ by

$$-2\frac{\mathrm{d}}{\mathrm{d}x}\left(\mu\frac{\mathrm{d}\hat{v}}{\mathrm{d}x}\right) = \frac{1}{2}\rho a^2. \tag{30}$$

The strain rate K is maximum at $x = -x_\delta$ and equal to $a = 2U/H$. Together with $K(0) = 0$, the strain rate K in the viscous boundary layer can be calculated. The velocity relation in the boundary layer is now equal to

$$u(x) = a x_\delta\left(\frac{x^3}{3x_\delta^3} + \frac{x^2}{x_\delta^2}\right), \tag{31}$$

with $x_\delta = 2\sqrt{\nu/a}$. The velocity profile in the burnt gas region has to be coupled to the velocity profile in the viscous boundary layer. The strain rate at $x = -x_\delta$ must equal $K = a = 2U/H$. Eq. (28) for $-H < x < -x_\delta$ now becomes:

$$u(x) = U - U\left(\frac{a(x + x_\delta/3)}{2U} + 1\right)^2. \tag{32}$$

We use the same approach to calculate the heat flux from the burnt gases to the glass product along a region close to the symmetry plane for the cylinder-symmetrical case as for the two-dimensional case. To calculate the heat flux for a non-viscous flow, the relation for the velocity (28) is substituted in the conservation equation (15). The heat transfer is now given by:

$$q = \lambda\left.\frac{\partial T}{\partial x}\right|_0 = \frac{\lambda(T_{(0)} - T_{\mathrm{flame}})}{H\int_{-1}^{0}\exp[-Pe(\frac{1}{3}x'^3 + x'^2)]\,\mathrm{d}x'}, \tag{33}$$

with $x' = x/H$. This relation can not be simplified using a Taylor expansion like for the two-dimensional case.

For a viscous flow, a distinction between the burnt gas region and the viscous boundary layer is made. For the viscous boundary layer, the relation for the velocity (31) is substituted in the energy Eq. (15), followed by the integration from $-x_\delta$ to 0. The relation for the velocity in the burnt gas region (32) is also substituted and now integration takes place from $-H$ to $-x_\delta$. After summation of these two terms, the heat flux is found:

$$q = \lambda\left.\frac{\partial T}{\partial x}\right|_0 = \frac{\lambda(T_{(0)} - T_{\mathrm{flame}})}{\mathscr{M}}, \tag{34}$$

with

$$\begin{aligned}\mathscr{M} = {} & H\int_{-x_\delta/H}^{0}\exp\left[\frac{1}{12}\frac{Pe^2}{Pr}x'^4 + \sqrt{\frac{4}{18}\frac{Pe^3}{Pr}}x'^3\right]\mathrm{d}x' \\ & + H\int_{-1}^{-x_\delta/H}\exp\left[-Pr - Pe\left(\frac{1}{3}x'^3 + \frac{1}{3}\sqrt{\frac{2Pr}{Pe}}x'^2\right.\right. \\ & \left.\left. + \frac{1}{9}\frac{2Pr}{Pe}x' + \frac{1}{9}\sqrt{\frac{2Pr}{Pe}}^3 + x'^2 + \frac{2}{3}\sqrt{\frac{2Pr}{Pe}} - \frac{1}{3}\frac{2Pr}{Pe}\right)\right]\mathrm{d}x'.\end{aligned} \tag{35}$$

4. Numerical results

4.1. Two-dimensional case

We use Fluent [24] to validate the results of the previous paragraphs. Fluent is a CFD (Computational Fluid Dynamics) package with which it is possible to carry out a numerical analysis and generate solutions of flow and heat transfer problems. Fluent uses a finite volume method and the flow calculations are based on the solution of the Navier–Stokes equations.

Fig. 5(left) shows a picture of a flame jet heating a quartz plate. The domain for the model used in Fluent is the layer just before the plate, represented at the right side of the figure. The flame is not modelled. A plug flow with a width of $2R$ impinges on a wall at a distance H. The inflow of the domain is an inlet boundary where the burnt gases enter the domain with a velocity of 75 m/s with a temperature of 3000 K. Like for the analytical model, the parameters of the burnt gases are chosen to be constant with

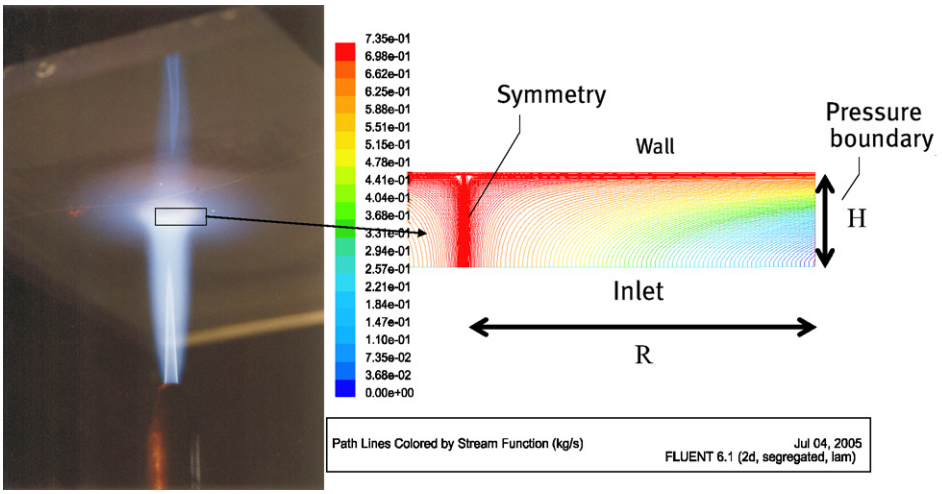

Fig. 5. Schematic overview of the Fluent model.

$\rho = \rho_b = 0.083\ \mathrm{kg/m^3}$, $c_p = 2000\ \mathrm{J/(kg\ K)}$, $\mu = 5.6 \times 10^{-5}$ kg/(m s) and $\lambda = 0.16\ \mathrm{W/(m\ K)}$. The values for c_p, λ and μ are chosen at a temperature of 1500 K using Chem1D [27] and the thermodynamic data from the GRI-mech 3.0 mechanism. The top side is a wall, which is fixed at the initial temperature of the glass being 300 K. The left side is a symmetry boundary and the right side an outlet-pressure boundary. Both the flow and the temperature fields are solved.

First we check the assumptions we made for the derivation of the analytical model. It was assumed that $\rho\frac{\partial u}{\partial x} > u\frac{\partial \rho}{\partial x}$ and therefore $K = -\frac{\partial u}{\partial x}$. Fig. 6 shows both terms plotted against x. For this particular calculation a temperature dependent density was used, namely $\rho = 1.1 \cdot (T/298)^{-106}$ [27]. The figure shows that far from the plate $u\frac{\partial \rho}{\partial x} = 0$. Closer to the plate $u\frac{\partial \rho}{\partial x}$ is not negligible anymore, but $\rho\frac{\partial u}{\partial x}$ still is the leading term. Therefore, the assumption seems to hold.

In Fig. 7 the separate terms of Eq. (7) are plotted against x. Far from the wall, the viscous term indeed is not relevant and therefore there is a balance between the convection term, the source term and the constant $\rho_b a^2$. Very close to the wall, the convection term and the source term become zero and the negative diffusion term equals the constant $\rho_b a^2$. The solutions for the velocity profiles far from the wall and in the viscous boundary layer close to the plate were linked together at $-x_\delta$, which is approximately 0.1 mm. At x_δ there is a balance between the four terms, which is not taken into account in the derivation of the analytical solution. The results of the numerical calculations will show whether this assumption has a big influence on the velocity profile.

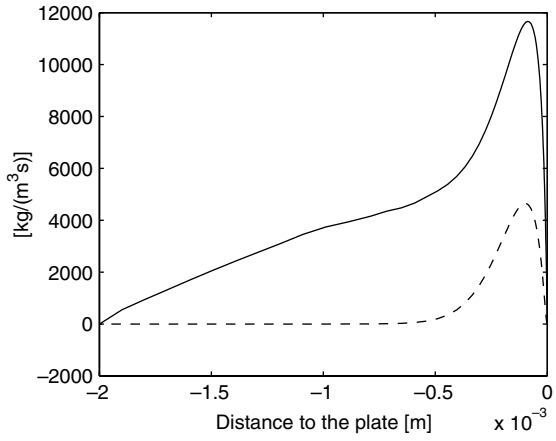

Fig. 6. The terms $-\rho\frac{\partial u}{\partial x}$ (solid line) and $u\frac{\partial \rho}{\partial x}$ (dashed line) plotted against the distance to the plate x.

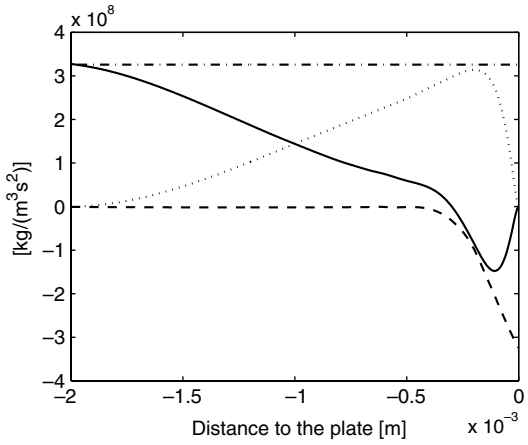

Fig. 7. The separate terms of Eq. (7). The solid line represents the convection term $\dot{m}\frac{dK}{dx}$, the dashed line the diffusion term $\frac{d}{dx}(\mu\frac{dK}{dx})$; the dotted line the source term ρK^2 and the dashed-dotted line the constant term $\rho_b a^2$.

The velocity profile of the burnt gases from the symmetry axis up to close to the edge of the stream tube when $H < R$ was derived earlier for the two-dimensional case. This velocity profile, Eq. (10) for the potential flow and Eqs. (13) and (14) for the viscous boundary layer, is compared with the numerical results of Fluent. The solution for a non-viscous flow with $\mu = 0$ is also compared. Fig. 8 shows the comparison between the analytical and numerical velocity profiles. The figure shows that the ana-

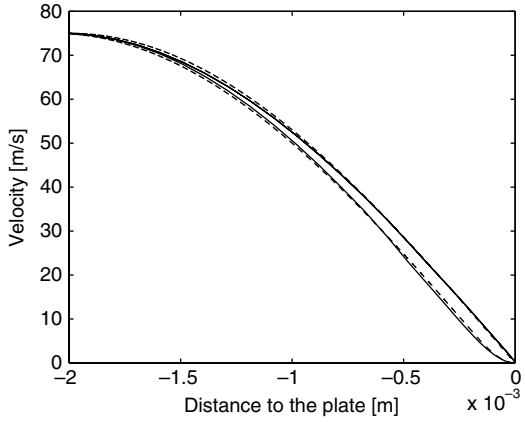

Fig. 8. Velocity profiles over the symmetry boundary for non-viscous (upper two curves) and viscous flows (lower two curves) for the two-dimensional case. The dashed lines represent the analytical calculations, the solid lines represent the numerical results.

lytical model corresponds very well to the numerical model in both cases.

The strain rate just before the plate determines the heat flux. A higher strain rate causes a smaller boundary layer and therefore a higher heat flux. We will now vary the strain rate a to determine its influence on the heat flux. With Fluent, contrary to the analytical model, it is also possible to calculate the velocity profiles if $H > R$, see Fig. 9. The width of the gas flow jet is $R = 0.5$ mm and the distance to the plate is varied from 4 to 1 mm. The figure shows that there is no visible difference in the velocity profiles for distances $H = 4$ or $H = 3$ mm. Decreasing the distance to $H = 2$ mm only has little influence on the flow near the plate, but if the distance is decreased to $H = 1$ mm, the velocity profile is visibly altered. The distance to the plate H has no influence on the velocity profiles for high H/R ratios, therefore the slopes of the velocity profiles will be the same. The strain rate of the burnt gas flow can only be increased if the distance to the plate H is decreased, i.e. if the ratio H/R is decreased. Since in this case the strain rate is increased, the heat flux from the burnt gas flow to the glass product is increased.

The results of the analytical model indicate that for small H/R ratios the strain rate is given by $a = \frac{\pi U}{2H}$. This relation no longer holds if the H/R ratio increases because of two-dimensional effects visible in Fig. 9. Fig. 10 shows the numerical effect of the H/R ratio on the effective strain rate of the burnt gases a. The factor $2aH/(\pi U)$ is set out as function of H/R. The figure shows that for small H/R values, $2aH/(\pi U)$ is equal to one. This observation is in agreement with the analytical solution. If the distance to the glass product H and the velocity U are kept constant and the width of the flow R is decreased, the effective strain rate a will increase. Furthermore, for a H/R ratio of 4 and higher and a fixed width of the flow R and velocity U, the distance to the glass product H has no influence on the strain rate a. The strain rate a now is a constant, represented by the straight line indicating that $\frac{2aH}{\pi U} \sim \frac{H}{R}$ or $a = \frac{\pi U}{2R}$ independent of H. The effect that for larger distances H no longer has an effect on the strain rate a, was also shown in Fig. 9.

The fitted line $2aH/(\pi U) = \frac{1}{2}H/R + \exp\left[-\frac{1}{2}H/R\right]$ predicts the numerical results quite accurately, see Fig. 10.

The temperature profile over the symmetry axis is also calculated with Fluent. The heat flux to the plate can be found from $q = \lambda \frac{\partial T}{\partial x}\big|_0$. The heat transfer is calculated for different Prandtl numbers, ranging from 0 (non-viscous flow) to 1.

Fig. 11 shows numerical and analytical results of these calculations for $H < R$. A distance to the plate of $H = 2$ mm and a plug width of $R = 20$ mm are chosen. The ratio of the viscous heat transfer and non-viscous heat transfer is plotted against Pr. The viscous heat transfer is calculated with Fluent for different Prandtl numbers and results are given by the asterisks. The non-viscous heat transfer is calculated with Eq. (16) as well. For a Prandtl number of 0, the ratio between the viscous heat transfer

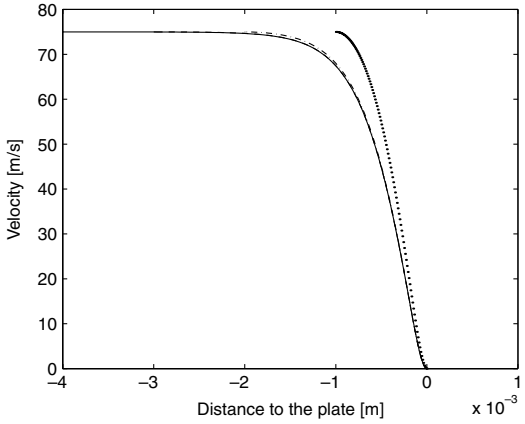

Fig. 9. Velocity profiles over the symmetry boundary for the two-dimensional case. For the solid line $H = 4$ mm, for the dashed line $H = 3$ mm, for the dashed-dotted line $H = 2$ mm and for the dotted line $H = 1$ mm.

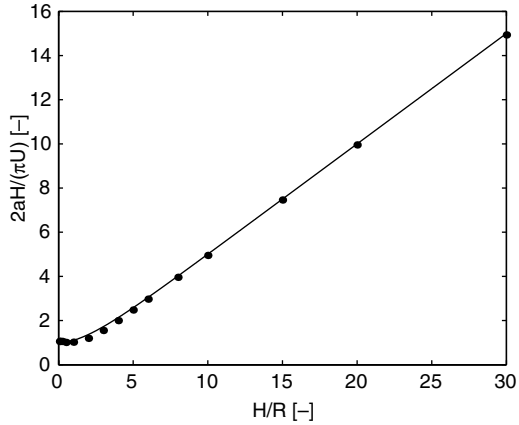

Fig. 10. Relation between $2aH/(\pi U)$ and H/R; the circles represent the numerical calculations, the solid line the fit function $y = \frac{1}{2}x + \exp\left[-\frac{1}{2}x\right]$, $x = H/R$ (two-dimensional case).

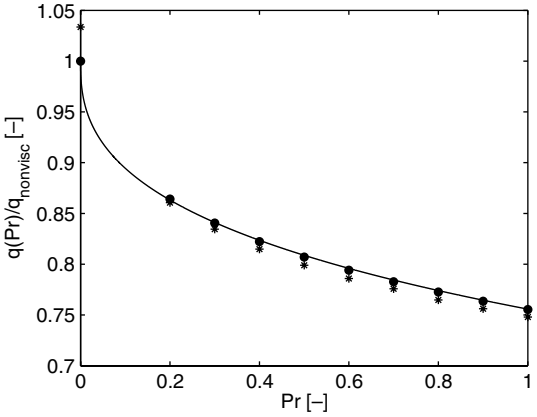

Fig. 11. The ratio of the viscous heat flux and non-viscous heat flux as a function of the Prandtl number. The dots represent the analytical results, the asterisks the numerical results; $H = 2$ mm, $R = 20$ mm (two-dimensional case).

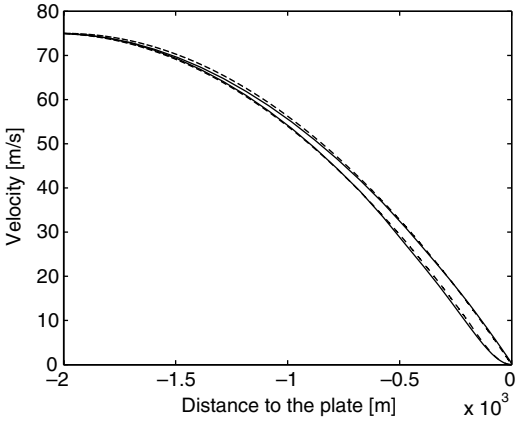

Fig. 12. Velocity profiles over the symmetry boundary for non-viscous and viscous flows for the cylinder-symmetrical case. The dashed lines represent the analytical calculations, the solid lines represent the numerical results.

and non-viscous heat transfer should be equal to 1. A small deviation can be observed. For increasing Prandtl number, the heat transfer should decrease due to an increasing viscous boundary layer thickness. The dots in the figure represent the ratio of the viscous heat transfer, calculated with Eq. (20), and the non-viscous heat transfer. As expected, the ratio equals 1 for a Prandtl number of 0.

The figure shows that the results of the analytical and numerical calculations show good agreements. By fitting a line through the analytical results, the heat transfer can be expressed as the non-viscous heat transfer multiplied by a function of Prandtl:

$$q = q_{\text{non-viscous}} \cdot f(Pr). \tag{36}$$

The fit function of Prandtl is given by $\exp[-0.28Pr^{0.40}]$. Combining this with Eq. (18), the heat transfer for the two-dimensional case can be expressed as:

$$q = \lambda \left.\frac{\partial T}{\partial x}\right|_0 = \lambda (T_{(0)} - T_{\text{flame}}) \frac{1}{H} \sqrt{Pe} \cdot \exp[-0.28Pr^{0.40}]. \tag{37}$$

4.2. Cylinder-symmetrical case

The same model is used as for the two-dimensional case, see Fig. 5. The velocity profiles calculated with the analytical model for $R > H$, Eq. (28) for non-viscous flows and Eqs. (31) and (32) for viscous flows, are validated with the Fluent calculations. Fig. 12 shows a good agreement between the analytical and numerical results again.

For small H/R ratios, the strain rate equals $a = \frac{2U}{H}$. For larger H/R ratios this relation for the strain rate a is not valid. Fig. 13 shows the effect of increasing H/R ratio on the strain rate a. The factor $aH/(2U)$ is plotted as a function of H/R. Indeed, for small H/R ratios, $aH/(2U)$ equals one, so the one-dimensional approximation is a correct one for $H/R < 1$. Keeping the distance to the plate H and the plug flow velocity U constant and decreasing the plug flow width R, results in an increasing strain rate a. Furthermore, for a H/R ratio of 4 and higher and a fixed plug flow width R and velocity U, the distance to the plate H has no influence on the strain rate a. This was also observed for the two-dimensional case. The numerical results are quite accurately predicted by the fitted line $aH/(2U) = \frac{18}{30}H/R + \exp\left[-\frac{18}{30}H/R\right]$.

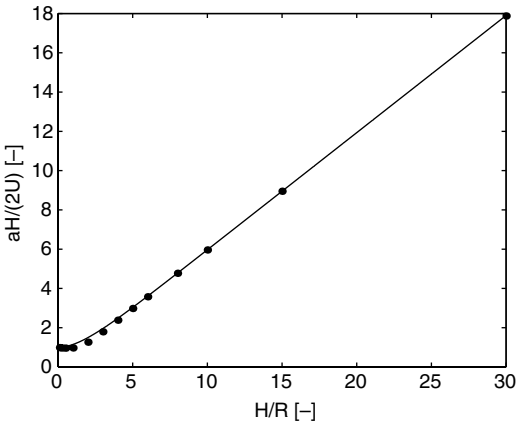

Fig. 13. Relation between $aH/(2U)$ and H/R; the circles represent the numerical calculations, the solid line the function $y = \frac{18}{30}x + \exp\left[-\frac{18}{30}x\right]$, $x = H/R$ (cylinder-symmetrical case).

To calculate the heat transfer to the plate, now a distance to the plate of $H = 2$ mm and a plug width of $R = 20$ mm are chosen. The asterisks in Fig. 14 represent the numerical calculations compared with the analysis. The ratio of the viscous heal transfer and the non-viscous heat flux is plotted against Pr. The non-viscous heat flux is calculated with Eq. (33), the viscous heat transfer with Fluent. Again, it can be observed that a small deviation occurs at $Pr = 0$ due to numerical inaccuracy; the ratio between the viscous and non-viscous heat flux is not equal to 1. The figure shows that for increasing Prandtl number the heat flux decreases due to an increasing viscous boundary layer. The dots represent the ratio of the viscous heat

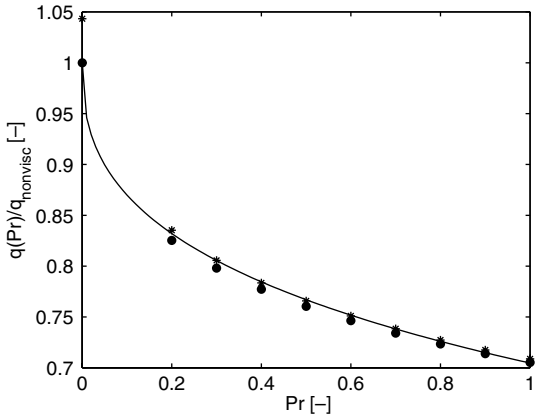

Fig. 14. The ratio of the viscous heat flux and non-viscous heat flux as a function of the Prandtl number. The dots represent the analytical results, the asterisks the numerical results (cylinder-symmetrical case). The results according to Sibulkin are represented by the triangles, with $R = 2H/\pi$.

transfer, calculated with Eq. (35), and the non-viscous heat transfer. The ratio equals 1 for a Prandtl number of 0.

The results of the analytical and numerical calculations show very good agreement. The heat transfer can be expressed as the non-viscous heat flux multiplied by a function of Prandtl. Therefore, a line is fitted through the analytical results: $f(Pr) = \exp[-0.35Pr^{0.40}]$. The heat transfer can now be expressed as:

$$q = \lambda \left.\frac{\partial T}{\partial x}\right|_2 = q_{\text{non-viscous}} \cdot \exp[-0.35Pr^{0.40}], \tag{38}$$

where $q_{\text{non-viscous}}$ is given by Eq. (33).

Sibulkin [20] solved the boundary layer equations for laminar heat transfer to a body of revolution near the stagnation point for the cylinder-symmetrical case. For the Nusselt number in the stagnation point he found:

$$Nu = 0.763\left(\frac{\beta}{\nu}\right)^{0.5} 2RPr^{0.4}, \tag{39}$$

where the Nusselt number is the ratio of convective to conductive heat transfer $Nu = h2R/\lambda$, with h the heat transfer coefficient [W/(m K)]. The velocity gradient just outside the boundary layer is defined here as $\beta = (\partial v/\partial r)_{r=0}$, see Fig. 4. This solution is independent of the flame tip-to-plate spacing. Furthermore, it is only applicable for larger spacing ($H/R > 8$) [21]. Since our analytical solution, Eqs. (34) and (35), is derived for closer spacing, $H < R$, we are not able to compare our results for the heat transfer with the ones found by Sibulkin. However, using Fig. 13, we can compare the velocity gradients. Kays found from potential flow solutions a velocity gradient for the cylinder-symmetrical case of $\beta = 2U/(\pi R)$ [22], while Kottke et al. experimentally determined a velocity gradient of $\beta = U/(2R)$ [23]. Fig. 13 shows that for larger spacing a constant strain rate of $a = 6U/(5R)$ can be found. Therefore, since $(\partial v/\partial r)_{r=0} = a/2$, see Eq. (24), the velocity gradient we find is equal to $\beta = 3U/(5R)$.

4.3. Validity range of the analytical solutions

The solutions we found for the heat transfer for the two-dimensional case (20) and (21) and the cylinder-symmetrical case (34) and (35) are valid for the hot spot of the plate, so for $y = 0$ to $y = R$, or $r = 0$ to $r = R$, respectively. With CFD calculations in Fluent we are able to see how the heat transfer decays with increasing distance to the symmetry plane.

The model we used in Fluent for these calculations is represented in Fig. 15. An isothermal plug flow with a temperature of $T = 3000$ K and a velocity of $U = 75$ m/s enters the domain at a distance H from the plate. The width of the plug flow is equal to $2R$. The hot gases flow out of the domain at a distance of $10R$ from the symmetry axis, to minimize the effect of the pressure boundary at the side on the plug flow. The top side is a wall and is fixed at a temperature of 300 K. The parameters of the burnt gases are the same as for the preceding calculations performed by Fluent.

The local heatflux at the wall is calculated for the two-dimensional as well as the cylinder-symmetrical case. Fig. 16 shows the ratio of the calculated heatflux and the analytical heatflux at the hotspot as a function of the normalized distance to the symmetry plane y/R for the two-dimensional case. The figure shows that at the symmetry plane the ratio of the numerical and analytical heatflux is almost equal to 1. The heatflux continuously decreases as

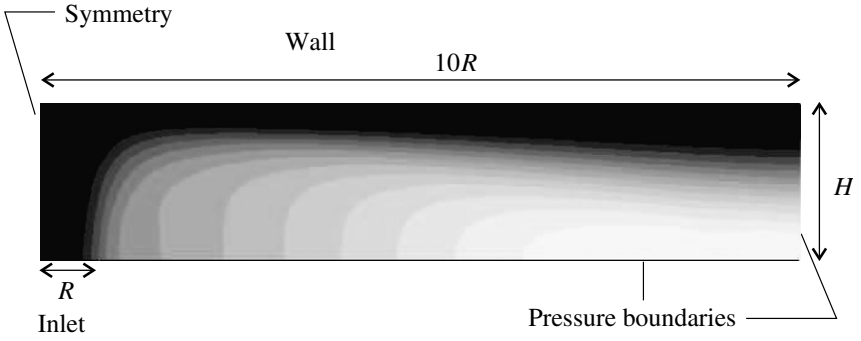

Fig. 15. Schematic overview of the Fluent model. The different grayscales represent the streamlines.

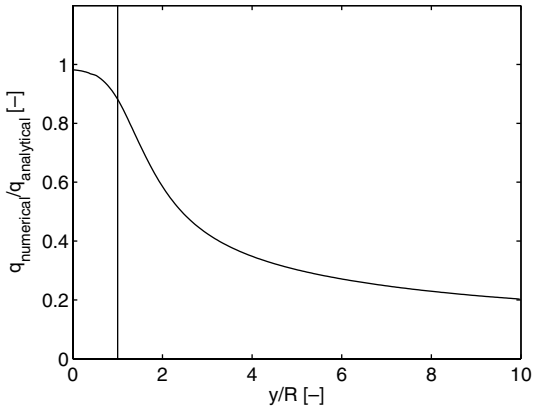

Fig. 16. Ratio of the numerically calculated heatflux and the analytical heatflux at the hotspot as a function of y/R for the two-dimensional case.

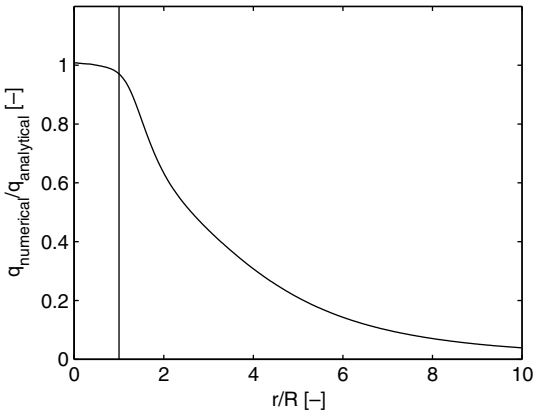

Fig. 17. Ratio of the numerically calculated heatflux and the analytical heatflux at the hotspot as a function of r/R for the cylinder-symmetrical case.

the distance to the symmetry plane increases. From a normalized distance of $y/R > 1$ a fast decay is observed.

The results for the cylinder-symmetrical case are shown in Fig. 17. Likewise, the ratio of the numerical and analytical heatflux is almost equal to 1 at the symmetry axis. Because the diverging gases have more directions to flow away from the axis, the strain rate and therefore the heatflux decreases less fast within the hotspot area compared to the two-dimensional case. From a normalized distance of $r/R > 1$ again a fast decay is observed. Therefore, for the two-dimensional as well as the cylinder-symmetrical case the analytical solutions for the heatflux seem to hold for the hotspot region. An error of atmost 10% is made at the edge of the plug flow for the two-dimensional case.

5. Conclusions

In this paper an analytical expression for the heat transfer of a flame jet to the hotspot with a width of $2R$ of a flat plate has been derived. It is shown that knowing the physical configuration, i.e. velocity of the flow, the distance from the flame tip to the plate, and width of the flow, the heat flux can be calculated in an easy way for the case that the flame is close to the plate. The flame jet is approximated by an isothermal flow and therefore the effect of chemical recombination is not taken into account.

The analytical expression is derived by taking into account only the dominant terms of the conservation equations. The derivation is done for a two-dimensional as well as a cylinder-symmetrical case. The geometry is divided in a region far from the plate to the viscous boundary layer, $-H < x < -x_\delta$, and a region from the viscous boundary layer to the plate, $-x_\delta < x < 0$. At x_δ, the solutions of the velocity profile close to the symmetry plane are linked to each other. The conservation equation of energy close to the plate is given by a balance between convection and conduction. Implementing the derived velocity relations into the energy equation and integrating over the domain results in a relation for the heat transfer to the hot spot of the plate.

The CFD package Fluent is used to validate the derived analytical expression with numerical calculations. The results of the calculations show that the assumptions hold with regard to which contributions of the conservation equations are most important in the different regions. The analytical expressions for the velocity profile close to the symmetry plane show very good agreement with the velocity profile calculated with Fluent. Also the heat flux calculated with the derived analytical expression show good agreement with the numerical calculations.

References

[1] Xianchang Li, J. Leo Gaddis, Ting Wang, Multiple flow patterns and heat transfer in confined jet impingement, Int. J. Heat Fluid Flow 26 (2005) 746–754.
[2] L.B.Y. Aldabbagh, I. Sezai, Numerical simulation of three-dimensional laminar multiple impinging square jets, Int. J. Heat Fluid Flow 23 (2002) 509–518.
[3] L.F.G. Geers, Multiple impinging jet arrays: an experimental study on flow hand heat transfer, Ph.D. thesis, Delft University of Technology, 2004.
[4] R. Viskanta, Heat transfer to impinging isothermal gas and flame jets, Exper. Thermal Fluid Sci. 6 (1993) 111–134.
[5] S.J. Wang, A.S. Mujumdar, A comparative study of five low Reynolds number k–ε models for impingement heat transfer, Appl. Therm. Eng. 25 (2005) 253–269.
[6] M. Angioletti, E. Nino, G. Ruocco, CFD turbulent modelling of jet impingement and its validation by particle image velocimetry and mass transfer measurements, Int. J. Therm. Sci. 44 (2005) 349–356.
[7] C.E. Baukal, B. Gebhart, A review of flame impingement heat transfer studies – Part 1: Experimental conditions, Combust. Sci. Technol. 104 (1995) 339–357.
[8] C.E. Baukal, B. Gebhart, A review of flame impingement heat transfer studies – Part 2: Measurements, Combust. Sci. Technol. 104 (1995) 359–385.
[9] C.E. Baukal, B. Gebhart, Heat transfer from oxygen-enhanced/natural gas flames impinging normal to a plane surface, Exper. Therm. Fluid Sci. 16 (1998) 247–259.
[10] T.H. van der Meer, Heat transfer from impinging flame jets, Ph.D. thesis, Delft University of Technology, 1987.
[11] S.G. Tuttle, B.W. Webb, M.Q. McQuay, Convective heat transfer from a partially premixed impinging flame jet. Part I: Time-averaged results, Int. J. Heat Mass Transfer 48 (2005) 1236–1251.

[12] S.G. Tuttle, B.W. Webb, M.Q. McQuay, Convective heat transfer from a partially premixed impinging flame jet. Part II: Time-resolved results, Int. J. Heat Mass Transfer 48 (2005) 1252–1266.
[13] L.L. Dong, C.W. Leung, C.S. Cheung, Heat transfer of a row of three butane/air flame jets impinging on a flat plate, Int. J. Heat Mass Transfer 46 (2003) 113–125.
[14] L.L. Dong, C.W. Leung, C.S. Cheung, Heat transfer and wall pressure characteristics of a twin premixed butane/air flame jets, Int. J. Heat Mass Transfer 47 (2004) 489–500.
[15] L.C. Kwok, C.W. Leung, C.S. Cheung, Heat transfer characteristics of slot and round premixed impinging flame jets, Exper. Heat Transfer 16 (2003) 111–137.
[16] L.C. Kwok, C.W. Leung, C.S. Cheung, Heat transfer characteristics of an array of impinging pre-mixed slot flame jets, Int. J. Heat Mass Transfer 48 (2005) 1727–1738.
[17] Z. Zhao, T.T. Wong, C.W. Leung, Impinging premixed butane/air circular laminar flame jet – influence of impingement plate on heat transfer characteristics, Int. J. Heat Mass Transfer 47 (2004) 5021–5031.
[18] C.E. Baukal, B. Gebhart, Surface condition effects on flame impingement heat transfer, Exper. Therm. Fluid Sci. 15 (1997) 323–335.
[19] M.F.G. Cremers, M.J. Remie, K.R.A.M. Schreel, L.P.H. de Goey, Heat transfer mechanisms of laminar flames of hydrogen + oxygen, Combust. Flame 139 (2004) 39–51.
[20] M. Sibulkin, Heat transfer near the stagnation point of a body of revolution, J. Aeronaut. Sci. 19 (1952) 570–571.
[21] P.S. Shadlesky, Stagnation point heat transfer for jet impingement to a plane surface, AIAA J. 21 (8) (1983) 1214–1215.
[22] W.M. Kays, Convective Heat and Mass Transfer, McGraw-Hill, New York, 1966.
[23] V. Kottke, H. Blenke, K.G. Schmidt, Messung und Berechnung des ortlichen und mittleren Stoffubergangs an stumpf angestromten Kreisscheiben bei unterschiedlicher Turbulenz, Wärme Stoffübertr. 10 (1977) 89–105.
[24] http://www.fluent.com.
[25] R.J. Kee, J.A. Miller, G.H. Evans, G. Dixon-Lewis, A computational model of the structure and extinction of strained opposed-flow premixed methane–air flames, in: 22nd Symposium (International) on Combustion, The Combustion Institute, 1989, pp. 1479–1494.
[26] G. Stahl, J. Warnatz, Numerical investigation of strained premixed CH_4–air flames up to high pressures, Combust. Flame 85 (1991) 285.
[27] http://w3.wtb.tue.nl/nl/organisatie/combustiontechnology/flamecodes/chem1d/.